Evaluation of change in pore network structure caused by halite crystallization

Etsuko Mizutani, Daisuke Ogura, Masaru Abuku, Hannelore Derluyn

EVALUATION OF CHANGE IN PORE NETWORK STRUCTURE CAUSED BY HALITE CRYSTALLISATION

Etsuko Mizutani[1,2*], Daisuke Ogura[3], Masaru Abuku[4] and Hannelore Derluyn[5,6]

KEYWORDS

Crystallisation, pore clogging, tortuosity, pore size distribution, image analysis

ABSTRACT

Pore clogging by salt crystallisation significantly changes both vapour and liquid moisture transport. This study aimed to quantify salt crystal distribution in porous materials and the change in the pore network structure before and after salt crystallisation to evaluate the effects of pore clogging on the mass transport phenomena. Three-dimensional scanning by synchrotron X-ray computed tomography (SPring-8, Japan) was conducted to quantify the time change in salt crystal distribution during evaporation. Fired clay brick specimens saturated with a salt (NaCl) solution were dried under ambient conditions and scanned at specific time instants. The amount of the salt crystal determined by image analysis was consistent with the estimated values obtained by the weight measurement of vaporised water. Additionally, the pore size distribution, tortuosity and effective porosity and specific surface area before and after salt precipitation are calculated by the 3D medial axis (3DMA) processing with segmented images to investigate the change of saturated hydraulic conductivity and vapour diffusivity due to salt precipitation. Below a certain depth, the physical properties decreased linearly with increasing salt occupancy.

1 NICH, Cultural Heritage Disaster Risk Management Center, Japan, mizutani02@tobunken.go.jp
2 NICH, Tokyo National Research Institute for Cultural Properties,Japan
3 Graduate school of Engineering, Kyoto University, Kyoto, japan
4 Kindai University, Higashiosaka, Japan
5 Universite de Pau et des Pays de l' Adour, E2S UPPA, CNRS, Total, LFCR, Pau, France
6 Universite de Pau et des Pays de l' Adour, E2S UPPA, CNRS, DMEX, Pau, France

1 INTRODUCTION

A prediction model for salt weathering is very useful for the development of appropriate conservation and restoration plans in various climatic conditions and several numerical models have been proposed [1,2]. However, there are many points where the physical phenomena related to salt precipitation in porous materials are still unknown.

One of the issues of improving the numerical analysis of salt weathering is how to express the change in mass transport properties due to the precipitation of salt. Although the significance of the effect of pore clogging due to salt precipitation on mass transport is apparent from experimental research in the literature [3, 4], the quantitative relationship between crystal formation and the change in the mass transport properties is unknown because of the difficulty of quantifying the salt crystals in the porous material. To relate salt precipitation and the change of transport properties, one should determine where and how much salts precipitate and how the salt crystals change the pore network structure. The pore network structure is mainly characterised by connectivity, pore size distribution and tortuosity, which are directly affecting gas and liquid transfer in porous media.

In this paper, a drying experiment using fired clay brick saturated with a NaCl solution is conducted to quantify the salt precipitation in porous media, as well as its influence on mass transport. Synchrotron radiation X-ray computed tomography (CT), which offers three-dimensional (3D) images with high spatial resolution, is used to quantify the spatial distribution of salt crystals through time in fired clay brick during drying. Additionally, the medial axis for void space before and after salt crystallisation is constructed in the 3D medial axis (3DMA)based on the burning algorithm [5] to calculate the pore size distribution, effective porosity, tortuosity and specific surface area. By using these parameters to characterise the pore network structure, the change of saturated hydraulic conductivity and vapour diffusivity due to salt crystals is directly calculated.

2 MATERIALS AND METHODS

2.1 Materials

Japanese fired clay brick (red brick produced by Okamoto Co.) was used for the experiments. The capillary moisture content of this brick is 0.17 m3/ m3, and the total open porosity is 0.24 m3/m3. Figure 1 shows the pore size distribution measured by mercury porosimetry.

Brick specimens of 5 mm × 5 mm × 8 mm were prepared, and an epoxy resin was applied on the lateral sides, making these surfaces water and vapour tight. This ensures a one-dimensional mass transfer during the drying experiments. Drying was monitored on three specimens after capillary saturating with a saturated NaCl solution. The monitoring was conducted both gravimetrically and through X-ray CT scanning at beamline BL20B2. The gravimetric measurements were performed outside of the X-ray CT hutch, at 25°C and 35.8 % RH, whereas the climate inside the hutch was slightly warmer, being 26.5°C and 33% RH on average. The specimens were placed in a holder as shown in Figure 2. The specimens were held by an upper polypropylene cup in which the salt solution was injected. Then the upper

cup was mounted in a lower cup with a saturated NaCl solution to suppress evaporation from the bottom surface of the sample.

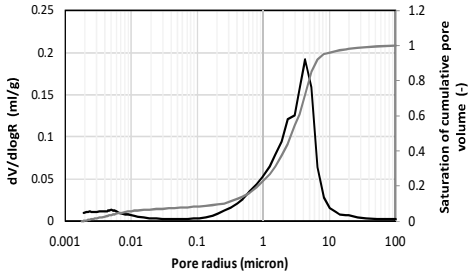

Figure 1: Pore size distribution of the brick sample at the beginning of the experiment measured by mercury intrusion porosimetry.

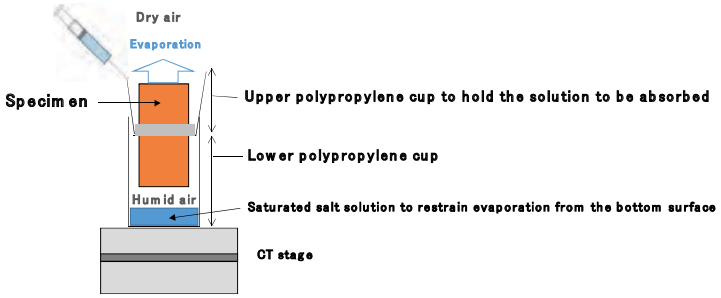

Figure 2: Schematic of the experimental setup.

2.2 Gravimetric experiments

The specimens were saturated with a salt solution by injecting the liquid into the upper cup with a syringe (Figure 2). The liquid was absorbed for 30 min. to ensure capillary saturation. Thereafter, the solution in the upper cup was wiped with a tissue, and the brick was dried via the upper surface of the test sample. The time curve of the accumulated amount of evaporation was measured with a balance with a 0.0001 g accuracy (Sartorius AG). Only the mass of the upper part, consisting of the upper polypropylene cup and the specimen, was measured so as not to be affected by the mass loss of the solution in the lower polypropylene cup. The mass was measured at intervals of approximately 15 min. during the initial stage of drying and, thereafter at 30 min. intervals.

2.3 X-ray CT experiments

Synchrotron radiation X-ray CT imaging was conducted at beamline BL20B2 (SPring-8, Hyogo prefecture, Japan) using a deflection electromagnet as a light source. The critical energy at BL20B2 is 28.9 keV, and the beam size is about 75 mm (horizontal) × 5 mm (vertical). A Hamamatsu Photonics' ORCAFlash4.0 CCD camera was used as the image detector. Scans were acquired with a spatial resolution of 2.74 μm/pixel, and the duration for one scan acquisition was approximately

5 min. The resulting 3D reconstructed volume of each scan consists of 2048 × 2048 × 1700 voxels (± 6.5 × 6.5 × 4.7 mm in width × depth × height).

First, a 3D CT scan of a dry specimen was conducted. After that, the specimen was wetted in the same way as for the gravimetric experiments, and the wet sample was imaged. Subsequently, several X-ray CT scans were conducted during the drying process, i.e. after 30, 60, 120, 180 and 480 min. of drying.

2.4 Image processing

The image processing starts with reducing the influence of noise, for which a median filter was used on the 3D reconstructed volumes of the brick specimen. The grey values of the CT images reflect the density and atomic number of the components present in the specimen. The specimen consists of solid brick and its pore space, which can be partly or fully filled with fluid (water or salt solution) and salt crystals. Each of these components has a different grey value distribution and by thresholding grey value ranges, the different components can be extracted, i.e. segmented, from the images. However, in our case, the overlap of the grey values of the substances is large. Therefore, the solid phase was segmented from the CT images of the dry brick and was subtracted from the images acquired during drying. The salt crystal phase was then segmented on the basis of the grey value thresholding of these differential images.

The segmented images are used for the construction of the medial axis for void space based on the burning algorithm [5] to calculate the pore size distribution, effective porosity, tortuosity and specific surface area. The 3DMA package for X-ray CT analysis has been used in the research field of soil science to characterise the pore structure of porous materials [6, 7]. In this 3DMA package, the void space is divided into nodal pores separated by throat surfaces. Each nodal pore was defined as the volume separated by throat surfaces. The equivalent pore diameter of each nodal pore is determined by assuming the pores are spheres. In this analysis, salt crystals are treated as solid to only deal with pores where liquid and gas flow occur. The analysis was conducted every 100 pixels (H) in the depth direction from the surface of the specimen (0 mm depth). Tortuosity is determined by summing the length of the medial axis voxels connecting the nodal pores lying on the opposite horizontal faces of the subvolume of 100 pixels in height and dividing this length by the straight-line distance between these faces.

3 RESULTS

3.1 Quantification of the time change of spatial distribution of salt crystals in porous media

The first step in this analysis was to evaluate the validity of the precipitated salt identification results obtained from the image analysis. The total open porosity of the whole sample identified by image analysis is 0.195 m3/m3, which corresponds to approximately 81% of the total open porosity of 0.240 m3/m3. This difference seems to be reasonable considering the ratio of voids below the spatial resolution (2.74 μm/pixel), as shown in Figure 1, that cannot be identified. Figure 3 shows the

comparison of the evolution as a function of the time of the total amount of precipitated salt obtained from gravimetry and CT image analysis. The amount obtained from gravimetry is calculated from the amount of water evaporation measured, assuming that salt crystals precipitate as soon as the salt concentration exceeds the saturated concentration. Although there would be some differences between specimens in Figure 3, the overall trend of salt precipitation can be rather sufficiently identified, which would confirm the suitability of the use of synchrotron X-ray CT imaging for verifying the temporal evolution of crystal formation in porous materials and its influence on the liquid transport phenomena.

Figure 4 shows the spatial distribution of salt crystals over time calculated by image analysis. Salt precipitation occurs mainly on the surface of the material for up to 120 min., and afterwards, salt precipitation progresses inside the material. It can be seen that salt precipitation occurs on the surface of the material in the early stage of the drying process when the capillary flow is dominant, and salt precipitation occurs inside the material in the later stage of the drying process when vapour diffusion is dominant [8,9]. To evaluate the change in pore structure due to pore crystallisation, the analysis of the pore network structure in the 3DMA was conducted for the segmented images at 180 and 480 min. as well as for the dry state.

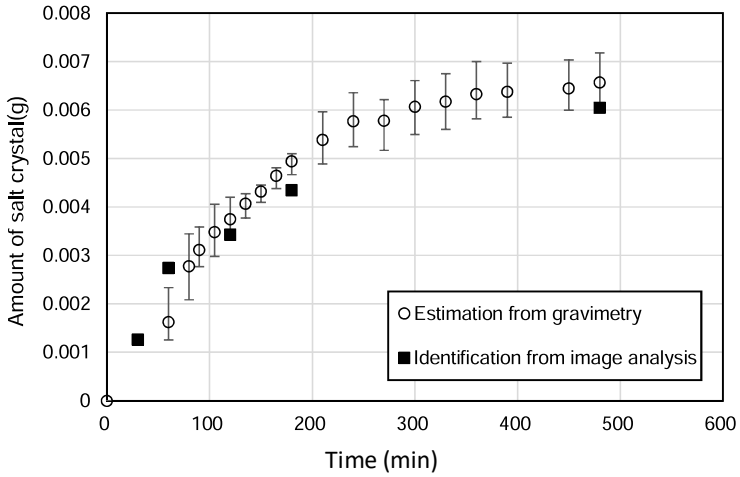

Figure 3: Total amount of precipitated salt as a function of time. The data points of estimation from gravimetry give the values averaged for the three specimens as well as the minimum and maximum values.

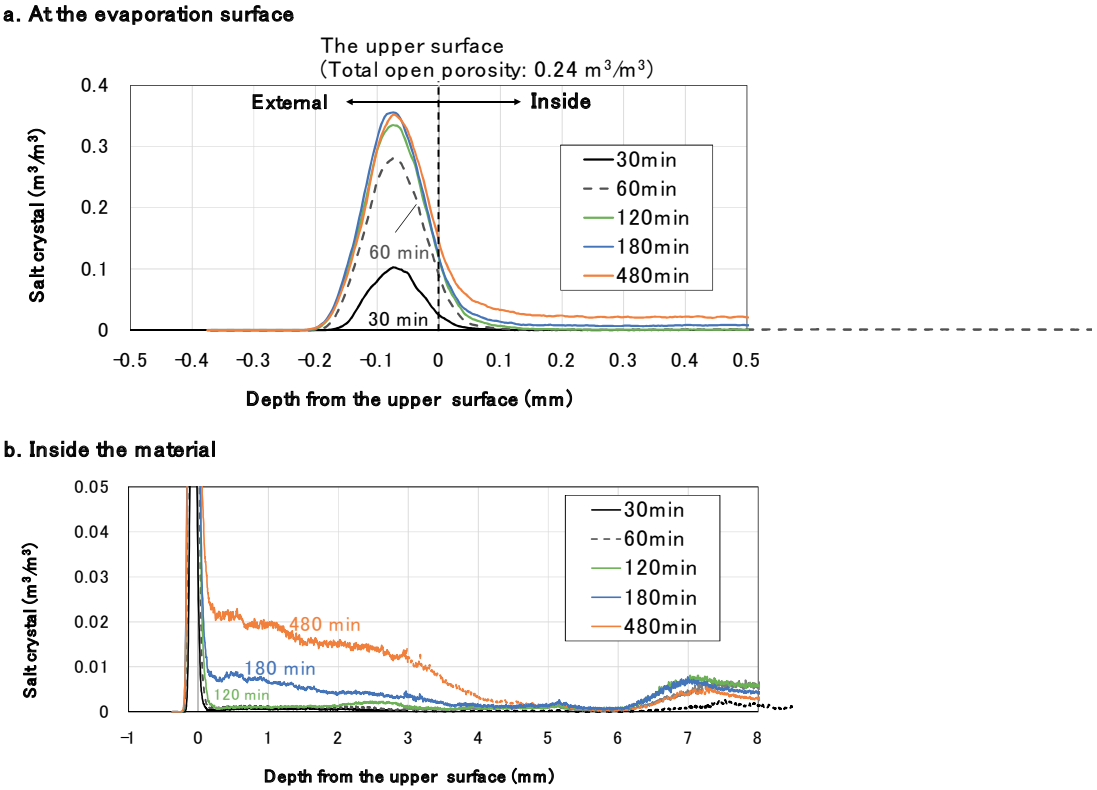

Figure 4: Spatial distribution of salt crystals over time.

3.2 Change of pore network structure due to salt crystallisation

Figure 5 shows the pore size distribution obtained from the 3DMA method at a depth of 0–0.274 mm from the top surface of the specimen. When compared to the result of the mercury injection method, the mean pore diameter value is shifted towards larger voids mainly because of the lack of spatial resolution. After 480 min., the number of pores decreased, but there was no significant change in the pore size distribution. Similar results were obtained by Todorovic's measurements[4] of the pore size distribution before and after sodium chloride precipitation using the mercury injection method. Therefore, although the evaluation of pore structure by image analysis has shown reasonable results, the limitation of its quantitative nature should be acknowledged because of the problem of spatial resolution. In the following, we will discuss the effect of salt precipitation mainly by comparing the results of the drying state and the state after salt precipitation.

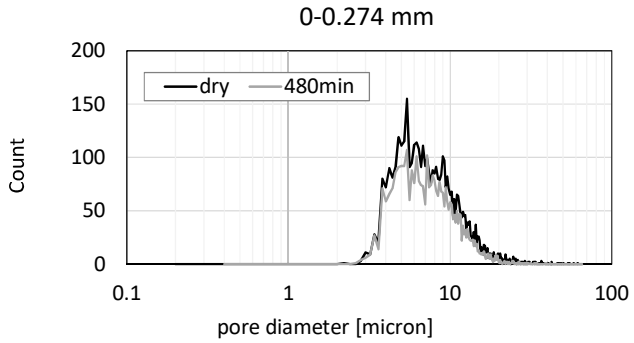

Figure 5: Pore size distribution calculated by 3DMA.

The changes in mass transport properties and pore structure due to salt precipitation are examined as changes in the salt crystal occupancy relative to the pore space Scr[-]. The salt occupancy Scr[-] is expressed as the ratio of the salt volume fraction to the total open porosity. Although many equations have been proposed to express the saturated hydraulic conductivity in soil physics, the Kozeny–Carman equation as shown in Equation (1) is used because it can be calculated directly from parameters characterising pore structure, where ψ_{eff} [m3/m3] is the effective porosity, Sv [cm−1] is the specific surface area, ρsol [g/cm3] is the density of the solution, η_{sol} [g/(cm ▪ s)] is the viscosity of the solution and g [cm s−2] is the acceleration of gravity. Equation (2) is the vapour diffusivity in porous media, which is expressed using vapour diffusivity in free air D_o [m2s−1], tortuosity τ and effective porosity.

$$K_{sat} = \frac{\psi_{eff}^3}{5S_v^2\left(1-\psi_{eff}\right)^2}\frac{\rho_{sol}g}{\eta_{sol}} \quad (1)$$

$$D_p = \frac{\psi_{eff}}{\tau^2}D_o \quad (2)$$

Figure 6 shows the degree of decrease in saturated hydraulic conductivity and vapour diffusivity associated with salt precipitation. The decrease in saturated hydraulic conductivity includes the effect of the change in the density and viscosity of the solution, with a maximum decrease of 0.31 (480 min., Scr = 0.21) times the value before precipitation. The decrease in the saturated hydraulic conductivity is mainly due to the decrease in the effective porosity caused by salt precipitation. Vapour diffusivity decreased down to 0.74 (480 min., Scr = 0.21) times the value before precipitation. The decrease in saturated hydraulic conductivity and vapour diffusivity is approximately linear with the increase in salt occupancy, except in the 0–0.247 mm region circled red in Figure 6, which is likely to be subject to pore clogging because of its proximity to the surface and large amount of precipitation. This result suggests the need for a different treatment depending on the depth from the surface or the amount of precipitation.

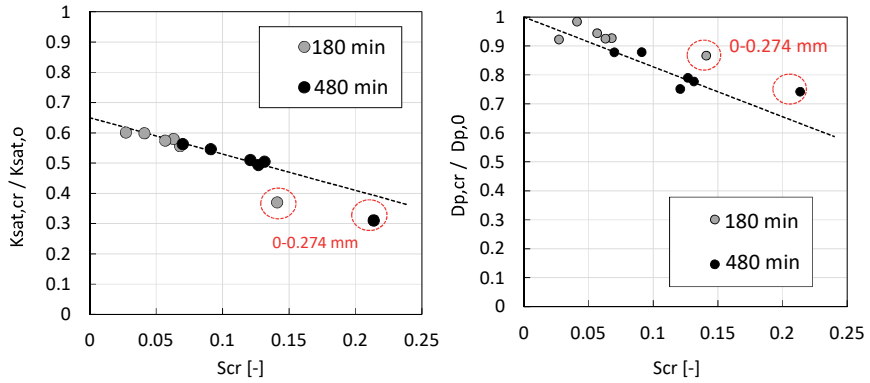

Figure 6: Decrease of saturated hydraulic conductivity and vapour diffusivity due to salt precipitation.

4 CONCLUSION

To elucidate the effect of the change of the pore structure associated with salt precipitation on the mass transport properties in fired clay brick, we quantified the amount of salt crystals and parameters such as pore size distribution, effective porosity, specific surface area and tortuosity by analysing images taken by synchrotron radiation X-ray CT during drying of specimen initially saturated with a salt solution. The validity of the identification of precipitated salt by image analysis was confirmed by comparing the amount of salt precipitation calculated from the weight loss of water. The pore size distribution, effective porosity, specific surface and tortuosity at the dry state, and after 180 and 480 min. of drying were calculated by the construction of the medial axis with the 3DMA package.

Using these parameters to characterise the pore structure, the saturated hydraulic conductivity and vapour diffusion coefficient could be directly calculated. Below a certain depth, the physical properties decreased linearly with increasing salt occupancy. These results provide important insights into the development of an appropriate expression of transport properties considering the change caused by salt-precipitation-induced pore clogging.

ACKNOWLEGEMENTS

This work was supported by JSPS KAKENHI Grant Numbers 16H06363, 18H01596, 19K23565 and 19H05511. H. Derluyn gratefully acknowledges the financial support from the European Research Council under the European Union's Horizon 2020 research and innovation programme (grant agreement No 850853). The synchrotron radiation experiments were performed at the BL20B2 of SPring-8 with the approval of the Japan Synchrotron Radiation Research Institute (Proposal No. 2018A1714 and 2018A1756).

REFERENCES

[1] M. Koniorczyk and D. Gawin, "Modelling of salt crystallization in building materials with microstructure - Poromechanical approach," *Constr. Build. Mater.*, vol. 36, pp. 860–873, 2012.

[2] H. Derluyn, P. Moonen, and J. Carmeliet, "Deformation and damage due to drying-induced salt crystallization in porous limestone," *J. Mech. Phys. Solids*, vol. 63, no. 1, pp. 242–255, 2014.

[3] R. M. Espinosa-Marzal and G. W. Scherer, "Impact of in-pore salt crystallization on transport properties," *Environ. Earth Sci.*, vol. 69, no. 8, pp. 2657–2669, 2013.

[4] J. Todorović and H. Janssen, "The impact of salt pore clogging on the hygric properties of bricks," *Constr. Build. Mater.*, vol. 164, pp. 850–863, 2018.

[5] W. B. Lindquist, S.-M. Lee, D. A. Coker, K. W. Jones, and P. Spanne, "Medial axis analysis of void structure in three-dimensional tomographic images of porous media," *J. Geophys. Res. Solid Earth*, vol. 101, no. B4, pp. 8297–8310, 1996.

[6] S. Hamamoto, P. Moldrup, K. Kawamoto, T. Sakaki, T. Nishimura, and T. Komatsu, "Pore network structure linked by X-ray CT to particle characteristics and transport parameters," *Soils Found.*, vol. 56, no. 4, pp. 676–690, 2016.

[7] M. Takahashi, U. Fujii, C. Ahn, T. Takemura, N. Takahashi, and H. Park, "Microstructure in Kimachi sandstone obtained with mercury intrusion porosimetry and μ-focus X ray CT structure analysis," *J. Japan Soc. Eng. Geol.*, vol. 52, pp. 184–191, 2007.

[8] G. W. Scherer, "Theory of Drying," J. Am. Ceram. Soc., vol. 73, no. 1, pp. 3–14, 1990.

[9] E. Mizutani et al., "Preliminary investigation of change of pore structure due to salt precipitation during evaporation in brick with X-ray computed tomography," in "Monument future : decay and conservation of stone - *Proceedings of the 14th International Congress on the Deterioration and Conservation of Stone*", 2020, pp. 455–460.